Solar magnetic fields and geomagnetic events.

Alexei A. Pevtsov[1] and Richard C. Canfield

Department of Physics, Montana State University, Bozeman, Montana

Short title: SOLAR MAGNETIC FIELDS AND GEOMAGNETIC EVENTS

Abstract.

Some interplanetary studies lead one to expect that the toroidal fields of individual active regions, whose solar cycle variations are described by the Hale-Nicholson hemispheric polarity law and the hemispheric helicity rule, are directly related to their heliospheric structure. In contrast, other interplanetary studies conclude that the large-scale solar dipolar field dominates the solar cycle modulation of the magnetic structure of interplanetary clouds. We have carried out two studies of solar magnetic fields and geomagnetic events that bear on these apparently conflicting views.

We first studied individual events within the period 1991 – 1998, during which the large-scale solar dipolar magnetic field pointed southward. We examined geomagnetic storms temporally associated with the eruption of 18 individual coronal X-ray sigmoids observed with the Yohkoh Soft X-Ray Telescope (SXT). We found that if a coronal flux rope model is used to interpret magnetic structure, eruptions with a southward leading magnetic field are associated with stronger geomagnetic storms, but those with a northward leading field are associated with more storms.

We next studied a much longer period, solar cycles 17-22, during which both the large-scale solar dipolar field and the active region polarities underwent three full magnetic cycles. We examined the temporal variation of the ratio of the geomagnetic A_p index to the sunspot number. We found no statistically compelling fluctuations of this quantity on solar-cycle time scales that are in phase with the reversal of active region polarities. On the other hand, we found a weak tendency for fluctuations that are in phase with the reversal of the large-scale solar dipole field.

From these two studies we infer that the magnetic structure of individual active regions plays a role in geomagnetic events, but their geoeffectiveness is complicated by asymmetries in the leading and following magnetic field and density. We conclude that simple cycle-dependent generalizations have only statistical significance, and cannot dependably be used to predict the geomagnetic effects of a given solar eruption.

1. Introduction

It is well understood that coronal mass ejections (CMEs) are responsible for major geomagnetic storms. However, some CMEs produce storms that are more significant than others. An important factor for geoeffectiveness is the orientation of the magnetic field. A prolonged southward component of the interplanetary magnetic field is necessary to trigger a major geomagnetic storm [*Gonzalez and Tsurutani*, 1987]. But how does this relate to magnetic fields at the Sun? In this paper we study the relationship between solar magnetic fields and geomagnetic storms.

CMEs are associated with various solar coronal phenomena, including eruptive filaments [e.g., *Gosling* et al., 1974] and long-duration X-ray events [e.g., *Gosling*, 1997; *Webb*, 2000]. At least half of all CMEs unambiguously identified with eruptions on the visible solar disk are associated with active regions [*Dere*, 2000; *Plunkett, 2000*]. One might therefore expect that the orientation of the magnetic field in interplanetary clouds associated with such CMEs will reflect two known tendencies of the photospheric magnetic fields of active regions: the Hale-Nicholson polarity law [*Hale and Nicholson* 1938] and the hemispheric helicity rule [e.g., *Martin et al.,* 1994; *Pevtsov et al.,* 1995]. The Hale-Nicholson polarity law describes the east-west component of active region magnetic fields, while the hemispheric helicity rule represents the north-south component. The Hale-Nicholson polarity law is solar cycle dependent, while the hemispheric helicity rule is not. Thus, if the CMEs carry out a significant part of the magnetic field of active regions, the interplanetary orientation of their fields will reverse

from one cycle to the next. This dependence on solar cycle is very graphically explained in Figure 2 of *Bothmer and Rust* [1997].

On the other hand, observational evidence that interplanetary cloud polarities tend to reverse with that of the large-scale dipolar field is found in work by *Zhang and Burlaga* [1988], *Bothmer and Rust* [1997] and *Bothmer and Schwenn* [1998], as well as recent studies reviewed by *Crooker* [2000]. *Mulligan et al.* [1998] showed that the magnetic structure of such clouds is modulated by the polarity of the large-scale dipolar field by showing that the direction of rotation of magnetic cloud fields reverses at the time of reversal of the large-scale solar dipolar field. This reversal typically takes place somewhat after solar maximum, whereas the field of active regions reverses at about solar minimum.

Finally, we note that no universal relationship appears to exist between the magnetic polarity structure of interplanetary clouds and their effectiveness for geomagnetic storms. The magnetic and density structure of an interplanetary magnetic cloud need not be axially symmetric, and that departure can apparently make either the leading polarity or the following polarity more geoeffective. *Fenrich and Luhman* [1998] showed that compression of the following part of the magnetic cloud can have a significant effect on geomagnetic storm intensity, if the magnetic field in that following part has a southward component. In their dataset only 45% of clouds showed compression of the following part, independent of magnetic field orientation in the cloud. Hence it is not surprising that one can easily find examples of clouds in which the leading part is significantly compressed. For example, in their study of five great magnetic storms, *Tsurutani et*

al. [1992] found two in which the driver gas (magnetic cloud) was compressed on the leading edge.

In this paper we describe two different studies of the relationship between the orientation of magnetic fields on the Sun and the magnitude of geomagnetic storms. In Section 2 we describe a study confined to solar X-ray sigmoids. *Canfield et al.* [1999] used Yohkoh SXT images of 61 active regions observed during 1993 and 1997 and classified them as eruptive/non-eruptive and sigmoidal/non-sigmoidal. They found that sigmoidal regions are more likely to be eruptive than non-sigmoidal ones. We find that sigmoids with southward leading interplanetary field (as inferred from a coronal flux-rope model) result in stronger storms than the sigmoids with northward leading field, but the latter are more numerous. This leads us to expect, at some level, a solar-cycle dependence of geoeffectiveness. In Section 3 we carry out a statistical study that covers more than six sunspot cycles, and show that the ratio of geomagnetic and sunspot indices exhibits no such solar-cycle dependence of geoeffectiveness. On the other hand, this study shows some dependence, whose statistical significance is unclear, on the polarity of the large-scale dipolar field. In Section 4 we discuss our results.

2. Erupting sigmoids and geomagnetic events.

2.1. Observations

Figure 1 shows two inverse-S sigmoidal active regions, one situated in the northern hemisphere (Figure 1a, AR 7790) and the other in the southern hemisphere (Figure 1c,

Figure 1

AR 7792). AR 7790 erupted on Oct. 19, 1994, when it was at $\sim$ N12W24. The eruption was accompanied by an M3.2 X-ray flare. AR 7792 erupted six days later, on Oct. 25, 1994, when it was at $\sim$ S08W12. An X-ray C4.7 flare was associated with this eruption. Geomagnetic events associated with these two eruptions are shown on Figure 2. Figure 1b and d show that although both sigmoids have inverse-S form, the polarities of the underlying photospheric magnetic fields are opposite. Is the difference in the geomagnetic responses to these two events related to their photospheric magnetic field orientation?

Figure 2

Using Yohkoh SXT images we identified 19 sigmoidal structures, such as those shown in Figure 1, whose eruptions (as inferred from coronal structural changes seen in SXT movies) were followed by geomagnetic storms within 5 days. Table 1 lists these sigmoidal regions, their approximate eruption times (the time of first SXT composite full-disk image that shows structural changes), their inferred leading polarity orientation (see Section 2.3 below), their active region number (if any), and the peak value of the A_p-index of the associated geomagnetic storm. For five events we were unable to identify the eruption that was associated with a given geomagnetic storm. For those regions Table 1 lists two possibly-related major eruptions. In one case, Nos. 10 and 11, we observed close eruptions in two different regions (AR 7315 and 7316), but only one geomagnetic storm. Since both regions had the same orientation of the magnetic field, as discussed below, we count this case only one eruption, and hence the following discussion contains only 18 cases.

Table 1

2.2. Models of coronal fields

Two fundamentally different magnetic field models have recently been used to model active regions whose structure is sigmoidal. The first is a *coronal flux-rope* (CFR) model, in which the active region magnetic field incorporates a helical structure like that of flux ropes seen in interplanetary clouds [*Gosling*, 1990, *Bothmer and Rust*, 1997]. In this model [*Titov and Démoulin,* 1999], a toroidal flux rope is embedded in a dipolar flux system. The projected magnetic separatrix surfaces are sigmoidal: S-shaped when the flux rope is right-handed and inverse S-shaped when it is left-handed. The alternative model uses a linear *force-free field* (FFF) [*Pevtsov et al.,* 1997]. In this model, the projected field lines in the core of the active region are sigmoidal (S-shaped when the force-free field parameter α is positive, and inverse-S structures when it is negative).

The key difference between these two models lies in their three-dimensional coronal structure and how it maps into the 3D interplanetary structure. Since we do not know how this mapping takes place, we simply hypothesize a self-similar expansion from the corona into the interplanetary medium, in the CFR case, and Gosling's [1999] picture of the formation of flux ropes from sheared arcades, in the FFF case. Figure 3 contrasts the CFR (left) and FFF (right) models, showing them as they would be seen in projection at the center of the solar disk. Both contain sigmoidal field lines, shown by the heavy inverse-S curves. The CFR cartoon in Figure 3a shows a left-handed flux rope as a simple cylinder joining two magnetic polarities; in this model, the sigmoid is formed by the projection of a separatrix surface [*Titov and Démoulin,* 1999]. In 3D, the

Figure 3

field lines at the apex of the coronal flux rope, which we assume will become the leading edge of the interplanetary cloud, have the longitudinal B_l and azimuthal B_a components shown in the figure. Figure 3b shows the alternative FFF model. In this model, the field lines in the core of the active region, which we assume will match the leading edge of the interplanetary cloud, have the inclination to the active region axis shown by $B_{\|}$. We therefore expect that as the coronal region expands into the interplanetary medium, and its axis rotates toward the ecliptic plane [e.g., *Wood et al.,* 1999], the leading field in the magnetic cloud will have a northward component in the CFR case, but a southward component in the FFF case.

2.3. Application of models to observations

Using Kitt Peak full disk magnetograms and the shape of the sigmoids (S or inverse-S), we inferred the direction (northward/southward) of the magnetic field in the leading part of each erupting sigmoid, using the two contrasting models discussed above in Section 2.2. For example, the photospheric magnetograms and the shape of the sigmoids shown in Figure 1 imply a northward leading magnetic field component for AR 7790 (Figure 1a) and a southward field for AR 7792 (Figure 1b), if we use the CFR model, but the opposite if we use the FFF model.

Table 1 shows the inferred leading-edge magnetic field orientation and corresponding Table 1
A_p index for the 18 sigmoidal structures using the two contrasting models. Adopting the CFR model for purposes of discussion, two effects are important.

First, Table 1 shows that the majority of the eruptions before 1996, solar minimum,

have northward leading fields. This tendency changed after solar minimum. This is simply a consequence of the Hale-Nicholson polarity reversal, which took place in 1996. It is important to remember that we determine the orientation of the leading field using solar magnetograms, not interplanetary observations. However, our data show that the relative frequency of strong storms increased after 1996. This increase is hard to understand in the framework of the results of *Mulligan et al.* [1998], since the orientation of the dipolar field was the same before and after 1996. Their work leads us to expect the change to occur after solar maximum, when the large-scale dipole field reverses, not solar minimum, when the leading polarity of active regions changes.

Second, we see from Table 2, showing the distribution of geomagnetic storms by orientation of the magnetic fields in sigmoids, that most storms are associated with northward leading fields, as *Fenrich and Luhman* [1998] showed. Again, this tendency is simply a result of the Hale-Nicholson polarity reversal at the end of solar cycle 22. Independent of that, however, events with southward leading fields in our data set tend to be associated with larger storms than those with northward fields.

Table 2

3. Solar cycle variation of the Geomagnetic A_p index.

In Section 2.3 we found that the frequency of larger storms increased after the time of the 1996 solar minimum, when the leading polarity of active regions changed. To determine whether a larger, more statistically significant database shows any changes associated with the Hale-Nicholson polarity reversal, we use on-line NGDC data for annually averaged sunspot numbers (S) and the A_p index as a function of time for the

last six solar cycles. Figure 4 shows that both parameters exhibit well-known solar cycle-related variations, although the correlation between the A_p index and S is not high ($\rho = 0.49$). Vertical dotted areas in the upper panel show approximate time periods in which the solar polar field reversals occur [*Harvey*, 1995], i.e., the approximate time of reversal of the polarity of the large-scale dipole. Dashed vertical lines in the lower panel show times of minima of solar activity, i.e., the approximate time when the magnetic fields of active regions reverse their polarity. We excluded ambiguous periods of multiple reversals (dotted areas) of the solar polar field from the following analysis.

Figure 4

We first consider the intervals between large-scale polarity reversals, i.e., between the dotted vertical bands in Figure 4. We compute the average A_p index and sunspot number for each of these intervals. The horizontal line segments in the upper panel of Figure 4 show the average A_p/S values during these intervals between large-scale polarity reversals. We see the value of the A_p/S ratio is always higher during periods in which the solar dipolar magnetic field is oriented *northward* (indicated by N) than during the adjacent periods when the field is oriented southward (S). The actual numerical values of the averages plotted in the upper panel are 1.00, .99, 1.00, 0.96, 0.97. All values fall within one standard deviation of the average, so we do not believe that the dependence is statistically compelling. However, it is consistent with the *Fenrich and Luhman* [1998] and *Mulligan et al.,* [1998] results, i.e., enhanced southward fields in the trailing parts of magnetic clouds leading to enhanced geomagnetic activity.

We then consider intervals defined by sunspot minima, i.e., between the dashed vertical lines in Figure 4. We compute the average A_p index and sunspot number

for each of these intervals. The horizontal line segments in the lower panel of Figure 4 show the average A_p/S values during these intervals, i.e., between active region leading-polarity reversals. There is no clear dependence of the averaged A_p/S ratio when the averaging is performed over formal solar cycles, as one would expect if the orientation of the interplanetary fields in magnetic clouds is cycle-dependent and either the leading or following edge of the magnetic cloud always dominates the geomagnetic effects.

4. Discussion

Our results lead to an obvious question. On the one hand, *in situ* observations of magnetic clouds show that the orientation of the magnetic field within them depends on the large-scale dipolar field of the Sun. On the other hand, many CMEs are associated with the solar active regions, whose magnetic field has certain orientation properties that are different from the large-scale dipolar field. The large-scale dipolar field of the Sun reverses its polarity after the sunspot maxima, but the leading sunspots of active regions reverse their polarity shortly after solar minimum. Which, if any, of these tendencies determine the cyclic variations of geomagnetic indices?

Our analysis of the relationship between the magnetic field orientation within sigmoids and the magnitude of geomagnetic storms (Table 2) reveals a preference for the sigmoids with southward leading field (CFR model) to produce stronger storms. On the other hand, the FFF model predicts oppositely directed northward field for the same events. Since both models correctly reproduce the shape of the sigmoids, neither

can be rejected without further discussion.

In Section 3, we studied the solar cycle dependence of geomagnetic activity (measured by A_p) relative to the sunspot number S. We found that the value of the A_p/S ratio is always higher during periods in which the solar dipolar magnetic field is oriented *northward* than during the adjacent periods when the field is oriented *southward*. This is consistent with the *Fenrich and Luhman* [1998] and *Mulligan et al.* [1998] results, i.e., enhanced southward fields in the trailing parts of magnetic clouds leading to enhanced geomagnetic activity in synchronism with the large-scale dipole field. However, it is not consistent with our results in Section 2, which show the leading polarity and relative frequency of strong storms changing after solar minimum.

We speculate that the cyclic variations of A_p/S depend on both the number of geomagnetic storms and their amplitude. We suggest that the dependence of A_p/S shown in the upper panel of Figure 4 is due to the modulation of weak (but much more numerous) geomagnetic storms by the dipolar field. On the other hand, Table 2 implies that the strong (but less frequent) storms reflect the polarity structure of their solar region of origin, whose leading polarity is southward in the CFR model. This speculation, however, is based on the orientation of the magnetic field derived using solar observations and the CFR model. We reject the alternative FFF model, since it cannot explain the solar cycle reversal in frequency of strong storms observed in 1996. This issue obviously needs further investigation using interplanetary measurements, to establish the relationship in magnetic field orientation between solar features and their associated interplanetary ejecta.

In closing, we emphasize what we believe is the most important result. Our observation show that in the time period 1991 – 1998 there is a clear tendency for sigmoids with leading southward fields to be associated with stronger geomagnetic storms (Table 2), and those with leading northward fields to be associated with weaker ones. This effect cannot be predicted on the basis of simple generalizations based on the phase of the solar cycle. Independent of interpretation, the orientation of erupting sigmoids can be determined using routinely available data (photospheric magnetograms and soft X-ray coronal images), and hence can easily be implemented in space weather forecasting.

Acknowledgments. The authors are pleased to acknowledge support by NASA through SR&T grant NAG5-6110 and the Yohkoh SXT contract NAS8-00119 at NASA Marshall Space Flight Center, and AFOSR through grant F49620-00-1-0128. NSO/Kitt Peak magnetic data used here are produced cooperatively by NSF/NOAO, NASA/GSFC and NOAA/SEL. Yohkoh is a mission of ISAS in Japan. The SXT instrument is a collaboration of the University of Tokyo, the National Astronomical Observatory of Japan, and the Lockheed Martin Solar and Astrophysics Laboratory.

References

Bothmer, V., and D. M. Rust, The field configuration of magnetic clouds and the solar cycle, in *Coronal Mass Ejections*, edited by N. Crooker, J. A. Joselyn, and J. Feynman, Geophys. Monogr. Ser., volume 99, pp. 139–146, AGU, Washington, D.C., 1997.

Bothmer, V., and R. Schwenn, The structure and origin of magnetic clouds in the solar wind, *Annales Geophyisicae, 16*, 1–24, 1998.

Canfield, R. C., H. S. Hudson, and D. E. McKenzie, Sigmoidal morphology and eruptive solar activity, *Geophys. Res. Lett., 26*, 627–630, 1999.

Crooker, N.U., Solar and heliospheric geoeffective disturbances, *J. Atmospheric and Solar-Terrestrial Res.*, in press, 2000.

Dere, K. private communication, 2000.

Fenrich, R. R. and Luhmann, J. G., Geomagnetic Response to Magnetic Clouds of Different Polarity *Geophys. Res. Lett., 25*, 2999–3002, 1998.

Gonzalez, W. D., and B. T. Tsurutani, Criteria of interplanetary parameters causing intense magnetic storms (Dst of less than -100 nT), *Planet. Space Sci., 35*, 1101–1109, 1987.

Gosling, J. T., Coronal mass ejections and magnetic flux ropes in interplanetary space, in *Physics of Magnetic Flux Ropes*, edited by C. T. Russell, E. R. Priest, and L. C. Lee, Geophys. Monogr. Ser., volume 58, pp. 343–364, AGU, Washington, D.C., 1990.

Gosling, J. T., Coronal mass ejections: an overview, in *Coronal Mass Ejections*, edited by N. Crooker, J. A. Joselyn, and J. Feynman, Geophys. Monogr. Ser., volume 99, pp. 9–16, AGU, Washington, D.C., 1997.

Gosling, J. T., The role of reconnection in the formation of flux ropes in the solar wind, in *Magnetic Helicity in Space and Laboratory Plasmas*, edited by Brown, M. R., R. C.

Canfield, and A. A. Pevtsov, Geophys. Monogr. Ser., volume 111, pp. 205–212, AGU, Washington, D.C., 1999.

Gosling, J. T., E. Hildner, R. M. MacQueen, R. H. Munro, A. I. Poland, and C. L. Ross, Mass ejections from the sun - A view from SKYLAB, *J. Geophys. Res., 79*, 4581–4587, 1974.

Hale, G. E., and S. B. Nicholson, *Magnetic observations of sunspots, 1917-1924*, Carnegie institution of Washington, Washington, D.C., 1938.

Harvey, K., Solar Polar Field Reversals, *e-mail,* ftp://ftp.ngdc.noaa.gov/STP/SOLAR_DATA/SUN_AS_A_STAR /Solar_Polar_Field_Reversals, 1995.

Martin, S. F., R. Bilimoria, and P. W. Tracadas, Magnetic field configurations basic to filament channels and filaments, in *Solar Surface Magnetism*, edited by Rutten, C. J. and C. J. Schrjiver, pp. 303–338, Kluwer Academic Publishers, Dordrecht, 1994.

Mulligan, T., C. T. Russell, and J. G. Luhmann, Solar cycle evolution of the structure of magnetic clouds in the inner heliosphere, *J. Geophys. Res., 25*, 2959–2962, 1998.

Pevtsov, A. A., R. C. Canfield, and A. N. McClymont, On the subphotospheric origin of coronal electric currents, *Astrophys. J., 481*, 973–977, 1997.

Pevtsov, A. A., R. C. Canfield, and T. R. Metcalf, Latitudinal variation of helicity of photospheric magnetic fields, *Astrophys. J., 440*, L109–L112, 1995.

Plunkett, S., private communication, 2000.

Titov, V. S., and P. Démoulin, Basic topology of twisted magnetic configurations in solar flares, *Astron. Astrophys., 351*, 707–720, 1999.

Tsurutani, B. T., W. D. Gonzales, F. Tang, and Y. T. Lee, Great Magnetic Storms, *Geophys. Res. Lett., 19*, 73–76, 1992.

Webb, D. F., The origins, propagation and space weather aspects of coronal mass ejections, *IEEE Transactions On Plasma Science, Special Issue on Space Plasmas*, in press, 2000.

Wood, B. E., M. Karovska, J. Chen, G. E. Brueckner, J. W. Cook, and R. A. Howard, Comparison of Two Coronal Mass Ejections Observed by EIT and LASCO with a Model of an Erupting Magnetic Flux Rope *Astrophys. J., 512*, 484–495, 1999.

Zhang, G. and L. F. Burlaga, Magnetic clouds, geomagnetic disturbances, and cosmic ray decreases, *J. Geophys. Res., 93*, 2511–2518, 1988.

A. A. Pevtsov, and R. C. Canfield, Department of Physics, Montana State University, Bozeman, MT 59717-3840. (e-mail: apevtsov@sunspot.noao.edu; canfield@physics.montana.edu)

Received _____

[1]Now at National Solar Observatory, Sunspot, New Mexico.

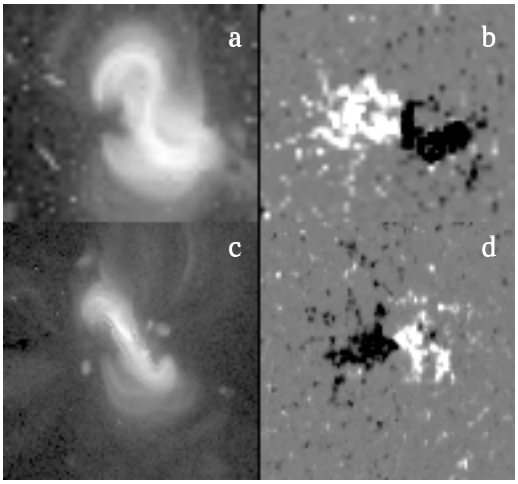

Figure 1. Sigmoidal coronal structures before eruption and their associated photospheric magnetic field. (a) - Yohkoh SXT image, AR 7790, 18-Oct-94, 15:51 UT, (b) - Kitt Peak magnetogram, AR 7790, 18-Oct-94, 15:47 UT, (c) - AR 7792, 25-Oct-94, 9:47 UT, (d) - AR 7792, 25-Oct-94, 16:06 UT. White corresponds to positive polarity magnetic flux, black to negative.

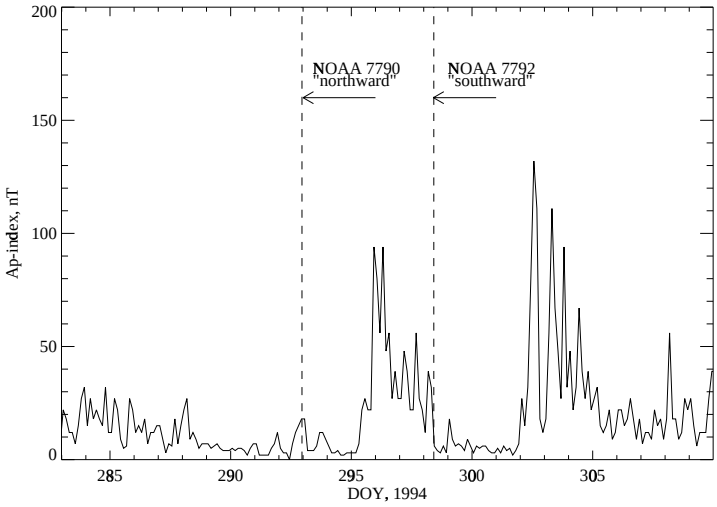

Figure 2. Geomagnetic storms associated with eruption of the coronal structures shown on Figure 1. Vertical dashed lines indicate approximate time of eruptions determined using Yohkoh SXT movies. The orientation of the magnetic field (northward/southward) specified in this figure is determined using the CFR model and Kitt Peak magnetograms.

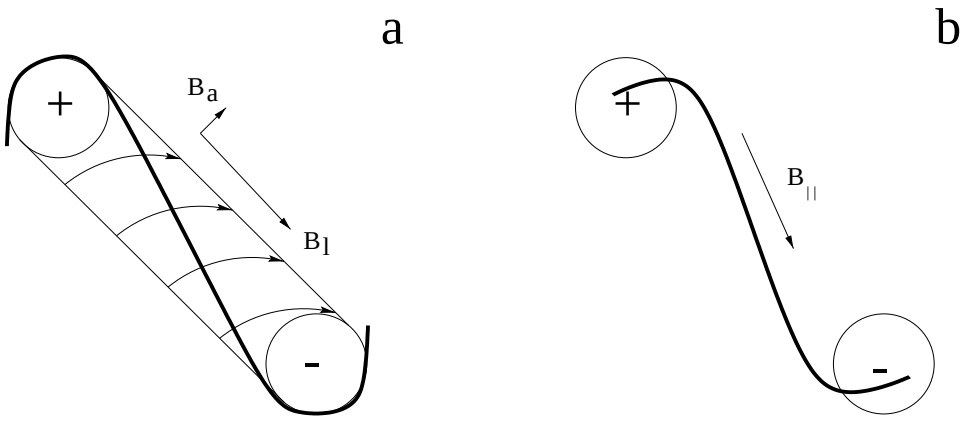

Figure 3. Two models of magnetic flux systems used to represent coronal sigmoids (thick inverse-S curves). (a) - coronal flux-rope (CFR) model and (b) - force-free field (FFF) model. Circles represent magnetic fluxes of positive (+) and negative (-) polarity. Thin lines connecting the two circles in (a) represent a flux tube projected onto the image plane, and curved arcs with arrows indicate the left-handed twist in the flux tube.

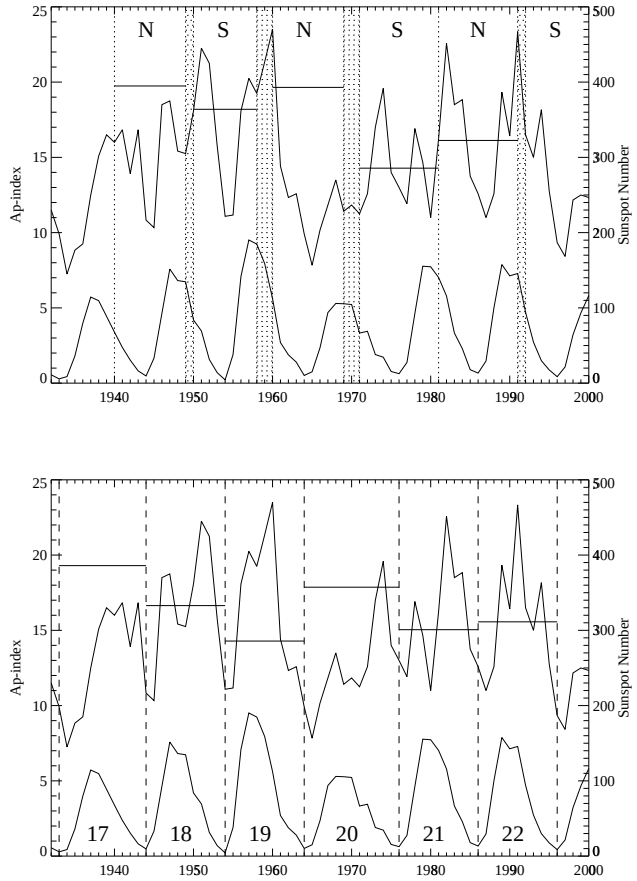

Figure 4. Both upper and lower panels show solar cycle-related variations of annual sunspot numbers (lower curve) and the geomagnetic A_p index (upper curve) for six solar activity cycles (17-22). Vertical dashed lines indicate solar minima. Vertical dotted lines and bands indicate times of polar field polarity reversals. The letters N and S in upper part of plot indicate the orientation of the solar dipolar magnetic field (northward/southward). Solid horizontal line segments show the cycle-averaged ratio (in arbitrary units, on a linear scale) of the A_p index to the sunspot number S for two different phases of solar activity: upper panel – A_p/S averaged over dipolar field cycles; lower panel – A_p/S averaged over solar cycles.

Table 1. Eruptions from sigmoids.

Eruption Number	SXT eruption Date (UT)	Orientation (CFR model)	NOAA AR	A_p index (peak)
1	1991/10/14 20:43	N	None	18
2	1991/12/26 17:08	N	6982	94
3	1992/02/06 09:34	N	7042	132
4	1992/03/16 20:07	N	7100	48
5	1992/03/28 22:13	N	7117	27
6	1992/04/08 08:19	N	7123	9
7	1992/05/08 15:04	S	7154	300
8	1992/06/17 14:42	N	7194	94
	1992/06/17 16:15			
9	1992/10/04 09:47	N	None	22
10	1992/10/22 07:42	N	7315	48
11	1992/10/22 15:35	N	7316	48
	1992/10/24 22:38			
12	1992/11/28 20:39	N	None	39
13	1992/12/24 04:20	N	7374	94
14	1994/10/19 22:55	N	7790	94

Table 1. (continued)

Eruption Number	SXT eruption Date (UT)	Orientation (CFR model)	NOAA AR	A_p index (peak)
15	1994/10/25 10:00	S	7792	132
16	1996/12/19 14:06	N	8005	22
	1996/12/19 15:30			
17	1997/04/07 13:29	S	None	111
	1997/04/09 14:16			
18	1997/05/11 23:11	S	8038	111
	1997/05/12 05:22			
19	1998/11/09 17:41	S	None	80

Table 2. Distribution of geomagnetic storms by orientation of the magnetic field in sigmoids.

Magnetic field orientation		Number of A_p storms within 5 days			
CFR model	FFF model	below 49 nT	50 – 99 nT	above 100 nT	Total
northward	southward	8	4	1	13
southward	northward	0	1	4	5